Research in Pharmaceutical Sciences, April 2026; 21(2): 146-163
Received: 27-8-025
Peer Reviewed: 18-10-2025
Revised: 29-10-2025
Accepted:01-11-205
Published:24-04-2026

School of Pharmacy & Pharmaceutical Sciences
Isfahan University of Medical Sciences

Original Article

Comparative evaluation of microfluidic-synthesized nano-niosomes versus liposomal and micro-niosomal deferoxamine in murine iron overload models

Ali Bazi[1], Somayyeh Karami-Mohajeri[2], Hajar Mardani Valandani[1], Elham Jafari[3], Fatemeh Oroojalian[4], Abbas Pardakhty[5,*], and Roohollah Mirzaee Khalilabadi[1,*]

[1]Department of Hematology and Medical Laboratory Sciences, Faculty of Allied Medicine, Kerman University of Medical Sciences, Kerman, Iran. [2]Department of Toxicology and Pharmacology, Faculty of Pharmacy, Kerman University of Medical Sciences, Kerman, Iran. [3]Pathology and Stem Cell Research Center, Kerman University of Medical Sciences, Kerman, Iran.[4]Natural Products and Medicinal Plants Research Center, North Khorasan University of Medical Sciences, Bojnurd, Iran. [5]Pharmaceutics Research Center, Institute of Pharmaceutical Sciences, Kerman University of Medical Sciences, Kerman, Iran.

Abstract

Background and purpose: Microfluidic technology provides enhanced standardization for formulating nanoencapsulated drugs compared to traditional bulk methodologies. Here, microfluidic nano-niosomal deferoxamine (Nn-DFO) was compared to micro-niosomal (Mn-DFO) and liposomal (L-DFO) formulations synthesized by conventional thin-film hydration.

Experimental approach: The formulations were subjected to physicochemical analyses. *In vivo* functional efficacy and safety were analyzed in mouse models of iron overload. Urinary and fecal iron excretion were also assessed.

Findings/Results: Mean particle sizes were 180.89±74.34 nm for L-DFO, 87.06±2.67 nm for Nn-DFO, and 7.41 ± 0.19 µm for Mn-DFO. Encapsulation efficiencies of L-DFO, Nn-DFO, and Mn-DFO formulations were 64.54%, 57.1%, and 70.72%, respectively. The 4-h drug release rates for L-DFO, Nn-DFO, and Mn-DFO formulations were 20.95%, 31.34%, and 26.30%, respectively, compared to 59.46% release from free DFO (F-DFO) within 4 h. Animals treated with F-DFO, L-DFO, Nn-DFO, and Mn-DFO showed significant reductions in the iron content of the liver (45.03%, 49.36%, 41.63%, and 23.52%, respectively). Urinary iron excretion on day 1st and fecal iron excretion on day 3rd after drug administration were the highest in the groups treated with F-DFO and Nn-DFO compared to other groups. Fecal iron excretion on day 7th was the highest in mice receiving Nn-DFO compared to different formulations.

Conclusion and implications: Nn-DFO synthesized by the microfluidic approach showed iron chelation efficacy and immediate iron excretion profile comparable to F-DFO, while being superior to Mn-DFO and L-DFO regarding delayed iron excretion.

Keywords: Drug carriers; Drug delivery systems; Iron chelating agents; Microfluidics.

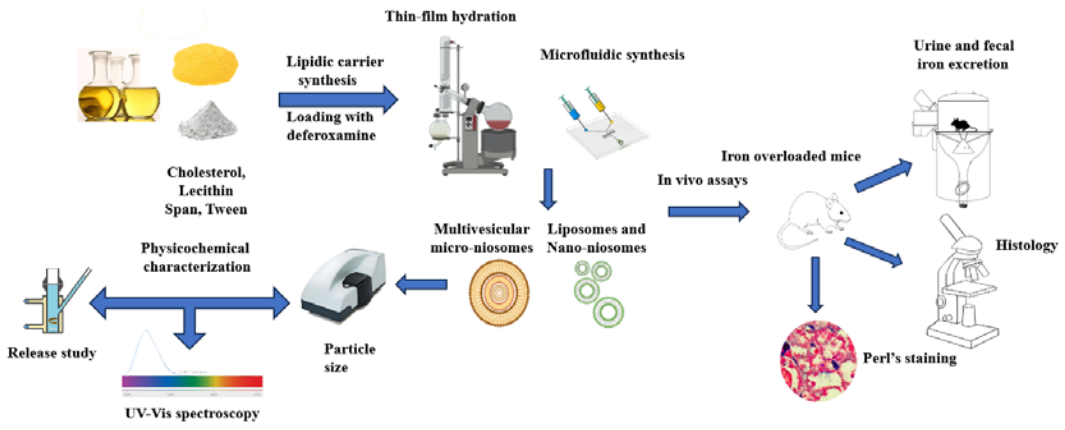

*Corresponding authors:
R. Mirzaee Khalilabadi, Tel: +98-, Fax: +98-
Email: r.mirzaee@kmu.ac.ir, khalilabadi60@gmail.com
A. Pardakhty, Tel: +98-3431325001-, Fax: +98-3431325002
Email: abpardakhty@kmu.ac.ir

Access this article online
Website: http://rps.mui.ac.ir
DOI: 10.4103/RPS.RPS_155_25

INTRODUCTION

Iron toxicity is a significant cause of morbidities (e.g., diabetes, renal failure, thyroid/gonadal abnormalities, and hepatic/cardiac failure) in patients suffering from iron overload conditions. Recent studies have shown that deregulated hemostasis of iron can also contribute to cerebral iron accumulation in neurological diseases such as Alzheimer's (1,2). Free iron is highly dangerous to living cells secondary to the generation of reactive oxygen species (ROS), leading to irreversible oxidation of vital biomolecules (proteins, lipids, etc) (3-5). The main iron chelators currently in use for defusing these problems include deferoxamine (DFO), deferiprone, and deferasirox (6). DFO has been the main and most effective iron chelator for decades, dating back to the mid-1960s when it was first approved in the United States (7). This hexadentate iron chelator offers the highest iron chelation activity among the three iron chelators listed; however, DFO faces some drawbacks that limit its clinical efficacy and patient adherence. For starters, the oral bioavailability of this chelator is extremely poor, so patients have to receive DFO *via* either the subcutaneous or intravenous route. For subcutaneous infusion, DFO needs to be continuously infused for over 8 to 12 h, which substantially compromises patient adherence. On the other hand, its intravenous administration has to overcome the risk of systemic toxicity and the short half-life of only about 20 min (4,6). The need for prolonged infusion is a key discouraging factor associated with poor adherence to DFO in patients with transfusion-dependent thalassemia and sickle cell disease (8). For these reasons, interests have grown toward slow-release and targeted nano-delivery systems for DFO (9,10).

Nano-based carriers have been widely employed to address the shortcomings of traditional forms of medications (11), including iron chelators and particularly DFO (12-14). These formulations, encompassing polymer-based carriers, dendrimers, micelles, nano gels, liposomes, and niosomes, generally aim to extend the bioavailability of DFO and obviate the need for its prolonged continuous administration. In recent years, niosomes have attracted the attention of researchers as a suitable and stable alternative to conventional liposomes (15). Although nano-carriers, including niosomes and liposomes, can be produced using different manufacturing approaches, the lack of scalability and reproducibility, as well as the time-consuming nature of conventional methods, limit the clinical use of these formulations (16,17). Other key issues that need to be answered when it comes to the clinical translation of nano-based drugs include safety, solubility, instability, off-target delivery, biocompatibility, clinical efficacy, and release kinetics. Extensive ongoing efforts try to address these limitations using novel modification/synthesis approaches, including microfluidic systems (18-20).

The microfluidics technology, a relatively new synthesis approach, has been recently applied to produce lipid-based nano-carriers (21). The main advantages offered by the microfluidic system include the use of small volumes of reagents, cost reduction, precise control over the synthesis process, time efficiency, homogenous reaction environment, and better adjustment of nanocarriers' physicochemical features (*e.g.*, shape, surface features, size) (22). The effective treatment of iron-overload conditions demands modified and optimized forms of iron-chelators that can obviate the limitations of their traditional forms (low bioavailability/therapeutic efficacy and undesirable pharmacokinetics and pharmacodynamic behavior, etc.). As noted, the microfluidic approach enables the resolution of limitations of conventional techniques (such as lack of reproducibility and standardization, being time- and cost-consuming, etc.). Despite previous efforts to develop nano-based carriers of DFO, no study has yet assessed the applicability of the microfluidic approach for preparing nano-formulations of this iron chelator. Regarding the increasing interest in lipid-based nano-DFO formulations, the goal of this study was to use the microfluidic technology to synthesize nano-niosomal DFO (Nn-DFO) and compare its physicochemical and functional features with liposomal (L-DFO) and micro-niosomal (Mn-DFO) formulations produced by conventional thin-film hydration.

MATERIALS AND METHODS

Materials

All materials used in this pilot study were of analytical grade. Span, Tween, Triton X-100, and cholesterol were from Fluka (Switzerland). Soybean lecithin was obtained from Carl Roth company (Germany). Deferoxamine mesylate was the product of Novartis Pharma (Switzerland). All other chemical reagents employed were of analytical grade and from Merck (Germany).

Liposome and micro-niosome preparation

Standard thin film hydration was utilized to prepare L-DFO and Mn-DFO. Liposomes composed of soybean lecithin and cholesterol (both at 50 mg/mL concentration in chloroform) mixed in the v/v ratios of 70:30, 60:40, and 50:50. Nine Mn-DFO formulations were produced using different ratios of cholesterol to Span and Tween 20, 40, and 60 non-ionic surfactants (cholesterol to Span/Tween ratios: 60:40, 50:50, and 70:30). The thin film was created using a vacuum rotary device at 70 °C, 100 rpm, for 40 min. During the hydration phase, 5 mL of 3 mg/mL DFO in phosphate-buffered saline (PBS, pH = 7.4) was added to the thin film, and rotation continued at 60 °C, 100 rpm for 30 min.

Nano-niosome preparation

First, the stock solutions (20 mg/mL) of non-ionic surfactants (Span/Tween 40) and cholesterol were prepared in ethanol using shaking and ultrasonication (1 min, 45 °C). DFO stock was prepared in PBS (3 mg/mL, pH = 7.4). Specific volumes of the regents were poured into glass containers and heated in a 45 °C bath. The lipidic phase was transferred into a 5 mL syringe, and the DFO-containing aqueous phase into a10 mL syringe. Nano-niosomes were generated using a microchip with the staggered herringbone mixer design and a nano-synthesis device (INSIGHT, NanoSynthes Co., Iran). A rotational flow of the two phases within the microchannels enabled the mixing and assembly of the two phases to form a nano-structured lipidic bilayer in a controlled manner. The ratio of the aqueous phase was 5 times that of the lipidic phase (5:1), and the total flow rate was 12 mL/min according to a previous report by Obeid *et al.* (20).

Morphology, size, and zeta potential analysis

Particle size analysis was performed using a particle size analyzer for Mn-DFO (Malvern Instruments, United Kingdom), and L-DFO and Nn-DFO formulations were analyzed by a nano-sizer (CORDOUAN Technologies, France). A zeta sizer device (Malvern Zeta-Sizer 3000, United Kingdom) was used to measure the surface charge of the particles. The morphology of Mn-DFO was checked under a light microscope equipped with an imaging system (Leica Biosystems, Germany), and Nn-DFO and L-DFO were visualized *via* field-emission electron microscopy (FE-SEM).

Encapsulation efficacy

In order to determine the encapsulation efficiency (EE) of lipid-based carriers prepared by thin film hydration (i.e., L-DFO and Mn-DFO), we used a specific volume of the formulation containing a known amount of the drug. After centrifugation at 13000 rpm for 30 min, the pellet was separated from the supernatant, and the concentration of the drug was determined in the supernatant by adding $FeCl_3$ (1.5 mM, ratio of 1:1 to a DFO-containing solution). The final amount of the drug was determined according to a standard curve and using equation 1. For Nn-DFO, EE was determined by pouring a specific volume of the formulation into a dialysis membrane, and then both sides of the membrane were sealed. The membrane was then inserted into a container with an appropriate volume of a solvent (PBS, pH = 7.4), and the drug was allowed to pass through the membrane on a stirrer. After 4 h, the concentration of the drug in the solvent and the membrane was determined. Isopropyl alcohol was used to dismantle vesicular particles (12).

$$\text{EE}\,(\%) = \frac{Total\ amount\ of\ DFO - free\ amount\ of\ DFO}{Total\ amount\ of\ DFO} \times 100 \quad \textbf{(1)}$$

Release kinetics

The release of DFO from niosomal and liposomal formulations was determined at 37 °C after 0, 15, 30, 60, 90, 120, 150, 180, and 240 min, as well as 6, 8, 12, and 24 h. The release profile of F-DFO was assessed until 8 h (the usual interval of infusion in clinical settings). For this purpose, the formulations containing DFO and F-DFO were passed

through a dialysis membrane into a known amount of the solvent (i.e., PBS). At specified times, 1 mL of the solvent was harvested and replaced with the same amount of fresh solvent to keep the final volume constant throughout the process. The amount of the drug released was then determined by adding $FeCl_3$ (1.5 mM, 1:1 ratio) and reading absorbance at 430 nm using a UV-Vis spectroscopy based on a standard curve. Finally, cumulative drug release and the kinetics of release were determined.

In vitro chelation activity

DFO was reacted with $FeCl_3$ (1.5 mM) at a 1:1 ratio. The complex formed following the reaction of DFO with ferric iron (i.e., ferrioxamine) was quantified *via* UV-Vis spectroscopy at 430 nm. The ability of niosomal and liposomal formulations to chelate iron *in vitro* was compared to that of F-DFO at the concentrations of 10, 20, 30, and 40 µg/mL. The chelation activity of F-DFO at each concentration was considered to be 100% (23).

Erythrocyte toxicity

The toxicity of formulations against erythrocytes was determined after incubation with a 5% red blood cell (RBC) suspension at 37 ℃ for 1 h. The concentrations used for this experiment were 10, 20, 30, and 40 µg/mL of the drug corresponding to the liposome/noisome concentrations of 1, 2, 3, and 4 µM, respectively. The percentage of hemolysis was determined by reading the absorption of the supernatant at 540 nm. Triton X100- and PBS-treated erythrocytes served as positive (100% hemolysis) and negative (0% hemolysis) controls, respectively.

Animals and grouping

Male adult mice (25-30 g) were obtained from the center for breeding of laboratory animals, Kerman University of Medical Sciences. The animals were kept under standard conditions with free access to water and food throughout the experiment. Housing and experimental protocols were approved by the Ethics Committee of Kerman University of Medical Sciences (Ethic code: IR.KMU.AEC.1403.034). A total of 18 mice were allocated to six groups (n = 3 per group), including negative control (normal saline), positive control (iron dextran), F-DFO (iron dextran + free non-encapsulated drug), L-DFO (iron dextran + liposomal drug), Nn-DFO (iron dextran + nano-niosomal drug), and Mn-DFO (iron dextran + micro-niosomal drug).

Model creation and interventions

The experiment included three phases. In the first four weeks, two mice in each group (except for the negative control group) received 50 mg/kg iron dextran intraperitoneally every other day. The second phase was a two-week washout period to allow iron redistribution. In the third phase, iron-overloaded mice (except for the positive and negative control groups) received five doses (50 mg/kg, every other day) of DFO formulations (F-DFO, L-DFO, Nn-DFO, and Mn-DFO) *via* intraperitoneal injections (24). A single mouse in each group was used to assess the toxicity of the formulations (two weeks, 50 mg/kg, every other day).

Urine and feces collection

After the injection of the fifth dose of the DFO formulations, the mice were transferred to metabolic cages to collect urine and feces samples on days 1st, 3rd, and 7th. Urine samples were collected in acidified microtubes to prevent iron deposition and kept at -20 ℃ until digestion. Feces were kept at room temperature.

Harvesting target tissues for histological analysis

At the end of the third phase and after collecting the last urine and feces samples, mice were scarified, and target organs (liver, heart, and kidneys) were collected and used for histological analysis, Perl's staining, and iron quantification. A slice of the liver, one kidney, and half of the heart, separated by a longitudinal cut, were immediately transferred into formaldehyde 10% for 24 h. After that, the samples were placed in a tissue processor and fixed with formalin, then dehydrated with alcohol, clarified with xylenol, embedded with paraffin, and finally underwent sectioning and staining with either hematoxylin and eosin (H&E) or Perl's (for visualization of iron deposits). Histological sections were assessed by an experienced pathologist blinded to the grouping.

Perl's staining

Ferrocyanide potassium was freshly prepared by dissolving 1 g of the powder in 25 mL of distilled water. The above solution was admixed with HCl solution in a 1:1 ratio and heated to 54 °C. Tissue slides were immediately immersed in this solution for 20 min. Afterwards, the tissue slides were gently rinsed with running water and stained with 1% neutral red for 15 s.

Iron quantification by atomic absorption spectroscopy

Samples (urine, feces, liver, and heart) were further analyzed for iron quantification using atomic absorption spectroscopy as previously described (25). First, the samples (urine: 300 µL, feces: 50 ± 10 mg, liver: 100 ± 5 mg, and heart: 100 ± 5 mg) were acid-digested using concentrated HNO_3 and HCl. Briefly, samples were transferred into microtubes, and then 1000 µL of concentrated HNO_3 was added to the microtubes, allowing for overnight tissue digestion. Next, concentrated HNO_3 and HCl (ratio of 3:1) were added to partially digested samples, and incubation was continued at 80 °C for 1 h. Then the samples were passed through syringe 0.22 µM filters and diluted using deionized water to a total volume of 5 mL. The samples were subjected to iron quantification *via* atomic absorption according to a standard curve in the range of 0.2-10 µg/mL.

Statistical analysis

Data were imported into Microsoft Excel 2019 for descriptive analyses. Inferential analyses were conducted in SPSS 16 software using one-way ANOVA and Bonferroni post-hoc test to compare liver and heart iron content, as well as urinary and fecal iron excretion between groups. Graphs were drawn using GraphPad Prism 8. Data are reported as mean ± SD.

RESULTS

Physicochemical properties of micro/nano niosomal and liposomal formulations

Particle size and morphology

Using thin film hydration, nine Mn-DFO formulations (F1-F9) were initially synthesized, encompassing a size range of 7.31 ± 0.83 to 43.87 ± 23.90 µm (Table 1). Regarding the average particle size, polydispersity index (PDI), size distribution curve, and morphology of micro-niosomes, the optimal formulation was chosen to be F5 (Span/Tween 40 with the ratio of 60:40 to cholesterol).

Table 1. The size distribution of micro-niosome, nano-niosome, and liposome formulations of deferoxamine that were synthesized using different ratios of cholesterol and non-ionic surfactants.

Formulations		MW (g/mol)		Molar ratio		Size (µm) Mean ± SD	PDI Mean ± SD
		S	T	S:T	S/T:Cholesterol		
Mn-DFO	F1	431	1310	1:1	30:70	7.31 ± 0.83	-
	F2	431	1310	1:1	40:60	57.57 ± 4.02	-
	F3	431	1310	1:1	50:50	14.27 ± 2.54	-
	F4	403	1282	1:1	30:70	7.41 ± 0.19	-
	F5	403	1282	1:1	40:60	9.04 ± 0.18	-
	F6	403	1282	1:1	50:50	9 ± 0.17	-
	F7	346	1226	1:1	30:70	19.24 ± 0.58	-
	F8	346	1226	1:1	40:60	7.76 ± 0.21	-
	F9	346	1226	1:1	50:50	11.11 ± 0.62	-
Nn-DFO		403	1282	1:1	40:60	87.06 ± 2.67	0.47 ± 0.01
		Soybean lecithin	Cholesterol	Soybean:Cholesterol		Size (nm)	
L-DFO	F1	758.08	387	40:60		180.89 ± 74.34	0.39 ± 0.05
	F2	758.08	387	50:50		231.18 ± 119.92	0.51 ± 0.04
	F3	758.08	387	70:30		261.45 ± 60.88	0.51 ± 0.03

Mn-DFO, Micro-niosomal deferoxamine; Nn-DFO, nano-niosomal deferoxamine; L-DFO, liposomal deferoxamine; S, Span; T, Tween; MW, molecular weight; SD, standard deviation; PDI, polydispersity index.

Using the optimal Span/Tween: cholesterol ratio obtained in thin-film hydration, Nn-DFO was constructed using the microfluidic technique, resulting in nanoparticles with a mean diameter of 87.06 ± 2.67 nm (PDI: 0.47 ± 0.01). Three L-DFO formulations with different ratios of lecithin to cholesterol retrieved the size range of 180.89 ± 74.34 to 261.45 ± 60.88 nm. The optimal liposomal formulation according to size distribution histograms was decided to be F1 (the lecithin: cholesterol ratio of 40:60). Regarding morphology, FE-SEM images of L-DFO (Fig. 1A) and Nn-DFO (Fig. 1B) showed uniform spherical nanoparticles, and Mn-DFO (Fig. 1C) appeared as well-formed uni- to multi-layered spherical structures.

Stability and zeta potential

Analyzing the size stability of the selected optimal formulations for up to 3 months revealed the acceptable stability of Mn-DFO (Fig. 2A), as well as L-DFO and Nn-DFO (Fig. 2B). The size distribution curves also verified the monodispersity of the formulations (Fig. 2C and D). The zeta potential values of L-DFO, Nn-DFO, and Mn-DFO formulations were obtained as -7.26, -38, and -3.45 mV, respectively.

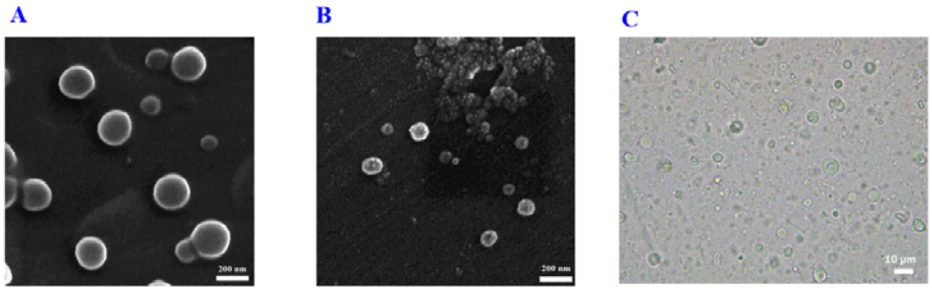

Fig. 1. Morphology of (A) liposomal, (B) nano-niosomal, and (C) micro-niosomal deferoxamine. All formulations showed spherical morphology with a good size distribution, as confirmed in dynamic light scattering.

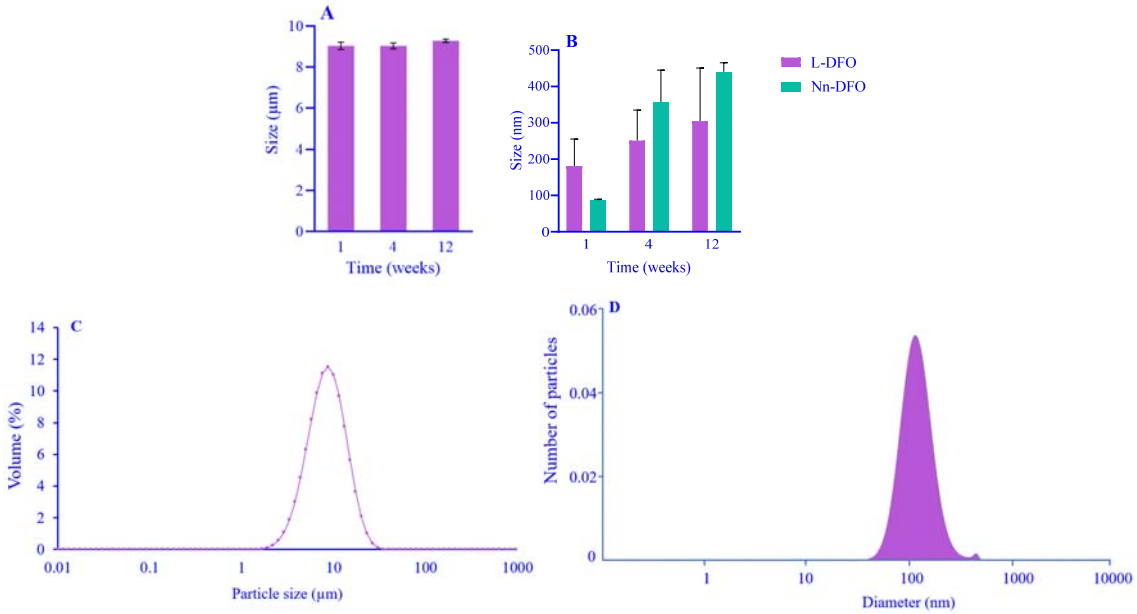

Fig. 2. Size distribution and stability of lipid-based formulations of deferoxamine for up to three months. (A) Mn-DFO, (B) Nn-DFO and L-DFO, (C) size distribution graph of Mn-DFO, (D) size distribution graph of L-DFO. Mn-DFO, Micro-niosomal deferoxamine; Nn-DFO, nano-niosomal deferoxamine; L-DFO, liposomal deferoxamine.

EE

For calculating the EE of the niosomal and liposomal formulations, we initially prepared a standard curve based on the formation of ferrioxamine (DFO-iron) complex and its distinct absorbance at 430 nm using a UV-Vis spectrophotometer. The results showed that the EE values for L-DFO, Nn-DFO, and Mn-DFO were 64.54%, 57.10%, and 70.72%, respectively.

Release kinetics

The amount of the drug released into the solvent across a dialysis membrane was measured *via* UV-Vis spectroscopy based on ferrioxamine absorbance at 430 nm. In the free form of the drug, 59.46 ± 1.14% of DFO passed through the dialysis membrane within 4 h; on the other hand, L-DFO, Nn-DFO, and Mn-DFO formulations released the chelator at the respective rates of 20.95 ± 7.36%, 31.34± 9.45%, and 26.30 ± 5.91% within 4 h (Fig. 3). According to data fitting parameters for DFO release respective to various models (Table 2), the best model predicting drug release behavior from L-DFO, Nn-DFO, and Mn-DFO was Korsmeyer-Peppas.

In vitro chelation and hemolytic activity

Chelation activity was assessed at four DFO concentrations of 10, 20, 30, and 40 µg/mL, showing that the encapsulation of DFO did not significantly compromise its chelation activity compared to the free form of the drug. Considering the activity of F-DFO as 100% at each dose, the lowest maintenance of chelating activity was related to L-DFO at 10 µg/mL (66.15 ± 15.06%) and the highest to Nn-DFO also at 10 µg/mL (92.88 ± 0.31%) (Fig. 4A). The highest rate of erythrocyte hemolysis (4.02 ± 2.39%) was observed in cells treated with 40 µg/mL of L-DFO for 1 h at 37 ℃ (Fig. 4B).

Table 2. Data fitting parameters for various models predicting deferoxamine release from liposomes, micro-niosomes, and nano-niosomes.

Deferoxamine formulations and release models		R^2	K	n
F-DFO	Zero order	0.6858 ± 0.0915	0.2954 ± 0.0454	
	First order	0.7475 ± 0.0914	0.0041 ± 0.0008	
	Higuchi	0.8316 ± 0.1056	3.9182 ± 0.5702	
	Korsmeyer-Peppas	0.7305 ± 0.2049	0.1347 ± 0.0676	0.1722 ± 0.0033
	Hixon-Crowell	0.7315 ± 0.0899	0.0056 ± 0.001	
L-DFO	Zero order	0.8243 ± 0.2097	0.1049 ± 0.0248	
	First order	0.8319 ± 0.2033	0.0011 ± 0.0003	
	Higuchi	0.8628 ± 0.0237	1.3131 ± 0.2404	
	Korsmeyer-Peppas	0.9539 ± 0.0044	0.0206 ± 0.0292	0.4433± 0.1960
	Hixon-Crowell	0.8295 ± 0.2055	0.0017 ± 0.0004	
Nn-DFO	Zero order	0.8408 ± 0.1536	0.1604 ± 0.0349	
	First order	0.8659 ± 0.1508	0.0018± 0.0004	
	Higuchi	0.9438 ± 0.0440	2.0655 ± 0.3913	
	Korsmeyer-Peppas	0.9723 ± 0.0121	0.0173 ± 0.0300	0.5233 ± 0.2269
	Hixon-Crowell	0.8580 ± 0.1520	0.0027 ± 0.0007	
Mn-DFO	Zero order	0.8474 ± 0.1394	0.1373 ± 0.0166	
	First order	0.8668 ± 0.1315	0.0015 ± 0.0002	
	Higuchi	0.9384 ± 0.0264	1.7644 ± 0.1640	
	Korsmeyer-Peppas	0.9705 ± 0.0165	0.0259 ± 0.0312	0.5631± 0.2748
	Hixon-Crowell	0.8606 ± 0.1343	0.0022 ± 0.0003	

F-DFO, Free deferoxamine; Mn-DFO, micro-niosomal deferoxamine; Nn-DFO, nano-niosomal deferoxamine; L-DFO, liposomal deferoxamine. Values represent mean ± SD from three release assay experiments.

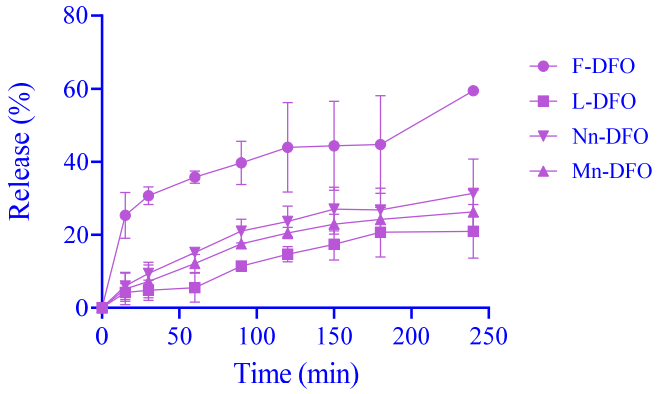

Fig. 3. Release kinetics of deferoxamine. Drug release was quantified in phosphate-buffered saline across a dialysis membrane at 37 °C over time (0, 15, 30, 60, 90, 120, 150, 180, and 240 min). F-DFO, L-DFO, Nn- DFO, and Mn- DFO showed a cumulative release of 59.46%, 20.95%, 31.34%, and 26.30%, respectively, during 240 min. F-DFO, Free deferoxamine; L-DFO, liposomal deferoxamine; Mn-DFO, micro-niosomal deferoxamine; Nn-DFO, nano-niosomal deferoxamine. Data represent mean ± SD from three replications.

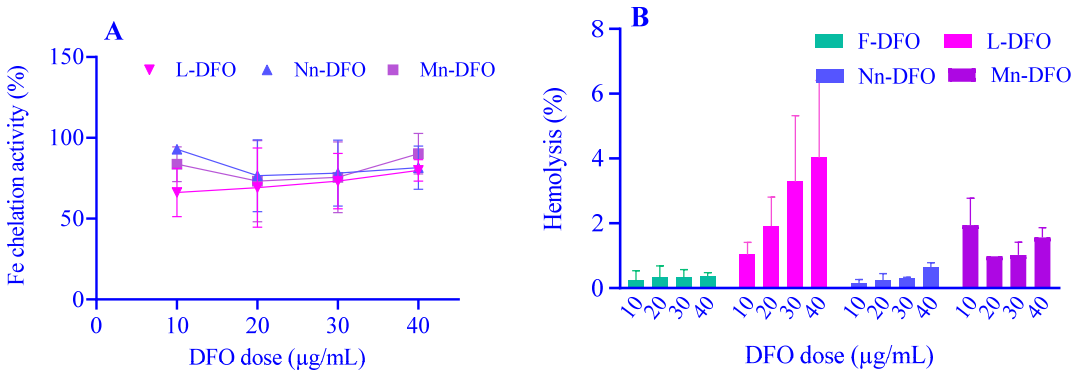

Fig. 4. *In vitro* chelation and hemolytic activity of free and encapsulated deferoxamine. (A) The chelation activity (%) of the drug encapsulated in L-DFO, Nn-DFO, and Mn-DFO compared to F-DFO, whose activity was considered 100% at each concentration. (B) Hemolysis of erythrocytes incubated with various deferoxamine formulations at 37 °C for 1 h. F-DFO, Free deferoxamine; L-DFO, liposomal deferoxamine; Mn-DFO, micro-niosomal deferoxamine; Nn-DFO, nano-niosomal deferoxamine. Data represent mean ± SD from two replications.

In vivo histological toxicity

The histologic evaluation of the liver in mice receiving different DFO formulations (Fig. 5) showed no significant histological lesions, except for mild to moderate degrees of lobular inflammation and Kupffer cell hyperplasia, compared to normal saline (Fig. 5A). In the iron dextran group (Fig. 5B), sinusoidal dilatation, portal vein congestion, and marked Kupffer cell hyperplasia were noticed. Focal mild lobular inflammation and degrees of Kupffer cell hyperplasia were seen in the liver in the F-DFO (Fig. 5C), L-DFO (Fig. 5D), and Mn-DFO (Fig. 5F) groups. In contrast, mild Kupffer cell hyperplasia was the only noticeable feature in the Nn-DFO group (Fig. 5E).

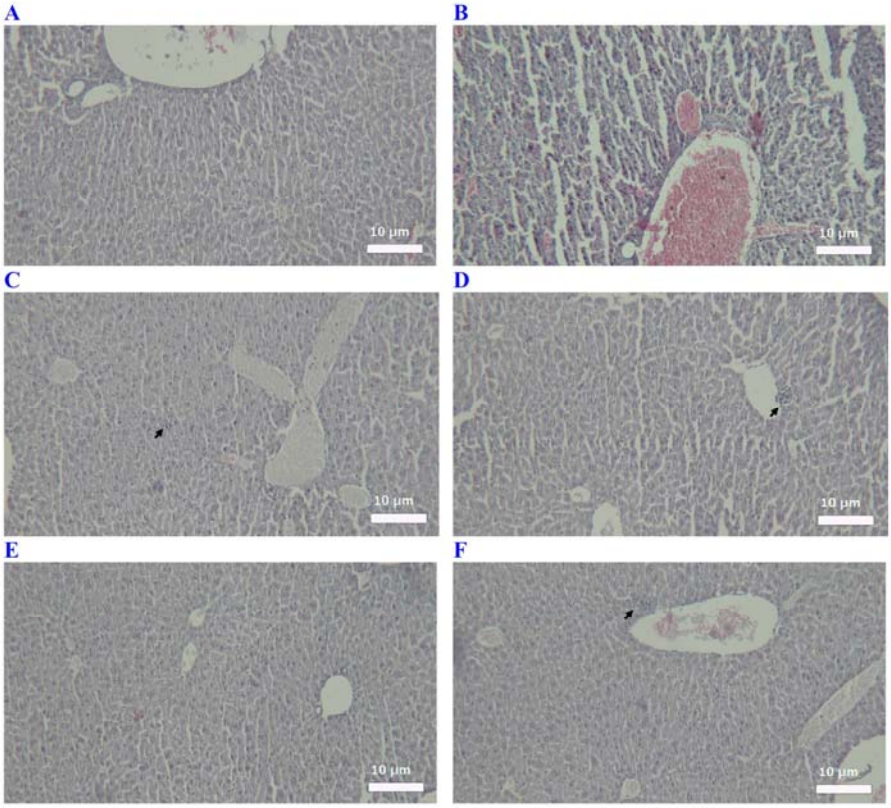

Fig. 5. Liver histopathology stained using hematoxylin and eosin. The animals were treated with either normal saline, iron dextran, or DFO formulations. Iron dextran and DFO formulations were infused for two weeks (50 mg/kg, every other day). (A) Normal saline: the liver tissue shows preserved architecture; (B) iron dextran: sinusoidal dilatation, portal vein congestion, and marked Kupffer cell hyperplasia were seen; (C) free DFO: preserved architecture with focal mild lobular inflammation (arrow) and moderate Kupffer cell hyperplasia; (D) liposomal DFO: preserved architecture, with focal mild lobular inflammation (arrow) and mild Kupffer cell hyperplasia; (E) nano-niosomal DFO: normal architecture with only mild Kupffer cell hyperplasia; (F) micro-niosomal DFO: preserved architecture with focal mild lobular inflammation (arrow) and mild Kupffer cell hyperplasia. Magnification: ×100. DFO, Deferoxamine.

In the kidneys (Fig. 6), no pathologic changes and normal glomeruli and tubules were observed in the normal saline group (Fig. 6A). Treatment with iron dextran (positive control) led to glomerular lobulation, focal mild infiltration by mononuclear cells, and slight tubular injury characterized by intratubular protein deposition (Fig. 6B). The F-DFO group showed normal glomeruli and tubules (Fig. 6C), and mild tubular infiltration by inflammatory cells was the only noticeable change in the L-DFO (Fig. 6D) and Mn-DFO (Fig. 6F) groups. In the Nn-DFO group, no pathologic changes were seen with normal glomeruli and tubules, and only mild vascular congestion (Fig. 6E).

In vivo efficiency

Histological liver sections were prepared for Perl's staining 10 days after the administration of the 5th dose of the formulations (Fig. 7). Mice infused with normal saline (Fig. 7A and 7G) revealed no iron deposits, while large block of iron deposits were frequently seen in the liver sections of mice treated with iron dextran for four weeks (Fig. 7B and 7H). Treatment with F-DFO (Fig. 7C and 7I), L-DFO (Fig. 7D and 7J), Nn-DFO (Fig. 7E and 7K), and Mn-DFO (Fig. 7F and 7L) considerably reduced iron deposition in the liver compared to the positive control.

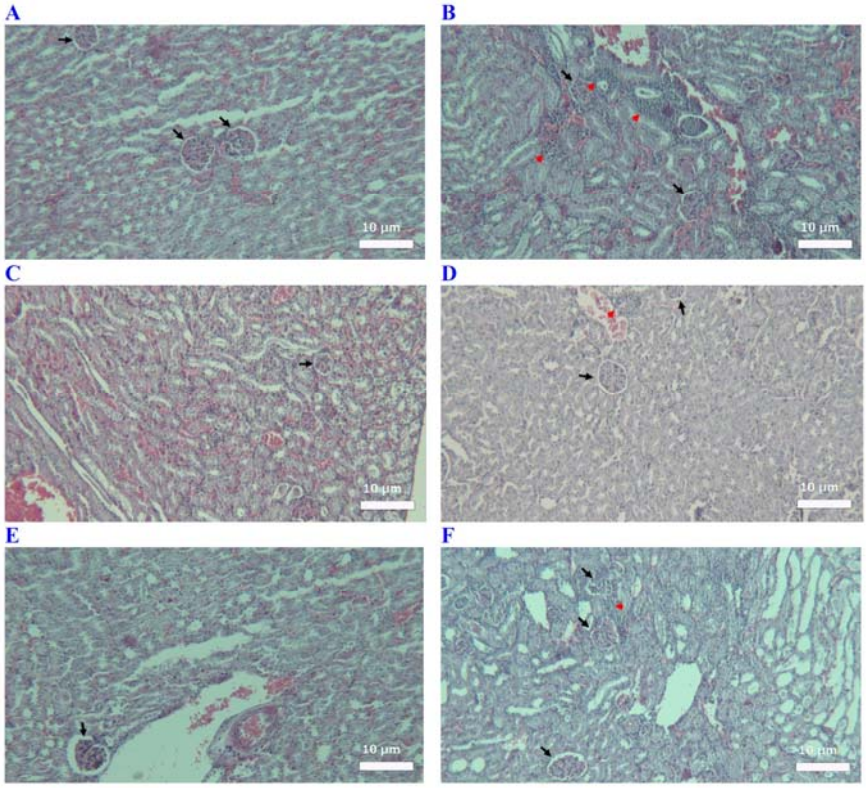

Fig. 6. Kidney histopathology stained using hematoxylin and eosin. The animals were treated with either normal saline, iron dextran, or DFO formulations for two weeks (50 mg/kg, every other day). (A) Normal saline: no pathologic changes, normal glomeruli (arrows) and tubules; (B) iron dextran: mild glomerular lobulation, focal mild mononuclear cells infiltration (red arrowheads) and mild tubular injury as intratubular protein deposition (black arrows); (C) free DFO: no pathologic changes, normal glomeruli (arrow) and tubules; (D) liposomal DFO: no significant pathologic changes, normal glomeruli (black arrows), tubules with mild chronic inflammatory cells (red arrowhead); (E) nano-niosomal DFO: no significant pathologic changes, normal glomeruli (black arrow), tubules with mild vascular congestion; (F) micro-niosomal DFO: normal glomeruli (black arrows) and tubules with only few chronic inflammatory cells (red arrowhead). Magnification: ×100. DFO, Deferoxamine.

Quantitative measurement of tissue iron revealed a significant reduction in the liver iron concentration of mice treated with various DFO formulations compared to the positive control (Fig. 8A). Also, cardiac iron concentration was significantly lower in the F-DFO, L-DFO, and Nn-DFO groups compared to the positive control (Fig. 8B). The rates of liver iron concentration reduction respective to positive control were 45.03%, 49.36%, 41.63%, and 23.52% in the F-DFO, L-DFO, Nn-DFO, and Mn-DFO groups (Fig. 8C), while cardiac iron concentration in these groups reduced by 31.02%, 33.39%, 34.77%, and 15.61%, respectively (Fig. 8D).

Urinary and fecal iron excretion

Regarding urinary iron excretion, a significant increase was observed in all groups receiving DFO formulations compared to the negative control group on the first day after the administration of the fifth dose (Fig. 9A), with the highest increase being observed in the F-DFO and Nn-DFO groups. On the third day, only the F-DFO group showed significantly higher urinary iron excretion compared to the saline group. No significant difference was seen between groups on day seven.

Fecal iron measurement on the first day revealed a significant increase in iron excretion only in the F-DFO group. On the 3rd day, the mice receiving F-DFO and Nn-DFO showed significantly higher fecal iron excretion compared to the control group. On the 7th day, mice receiving Nn-DFO showed significantly higher fecal iron excretion compared to the control group (Fig. 9B).

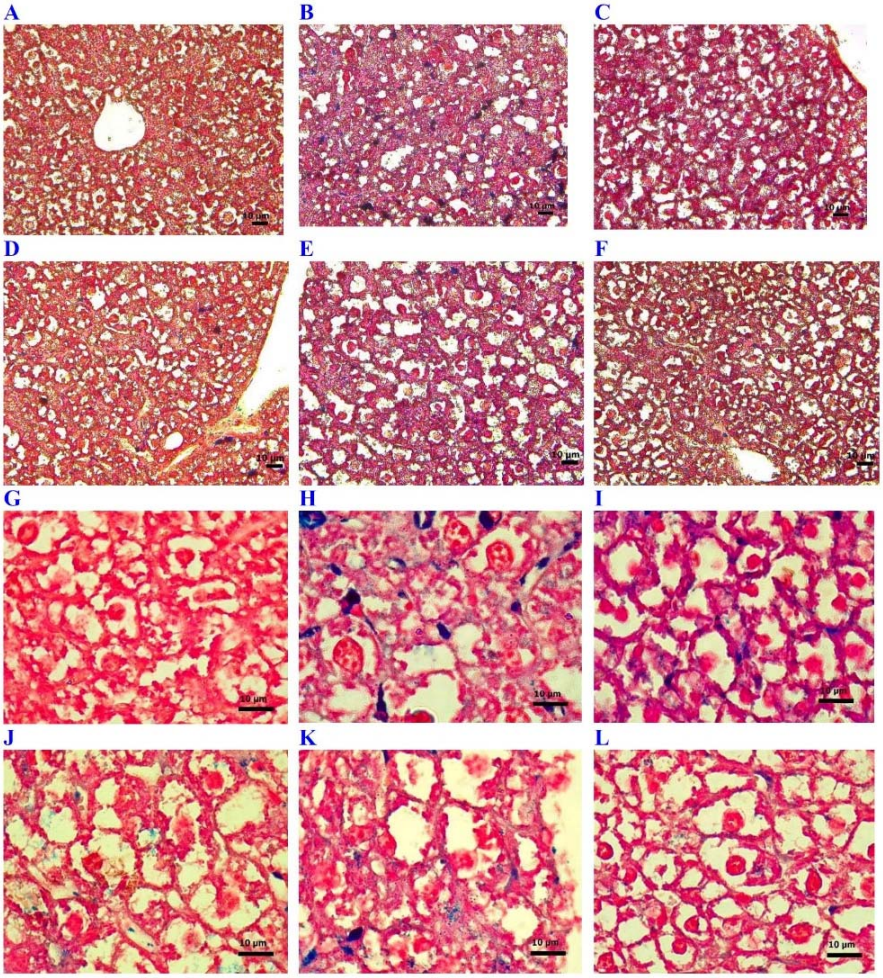

Fig. 7. Perl's staining of hepatic sections. (A and G) Negative control (normal saline) showing no iron deposits; (B and H) positive control: iron dextran (50 mg/kg, every other day, four weeks), showing large iron blocks as blue color deposits across all fields. The experimental groups receiving DFO formulations, including (C and I) iron dextran + free DFO; (D and J) iron dextran + liposomal DFO; (E and K) iron dextran + nano-niosomal DFO; (F and L) iron dextran + micro-niosomal DFO, showed reduced iron deposits in histological fields. Magnification of parts A-F: × 40 and for parts G-L: × 100. F-DFO, Free deferoxamine.

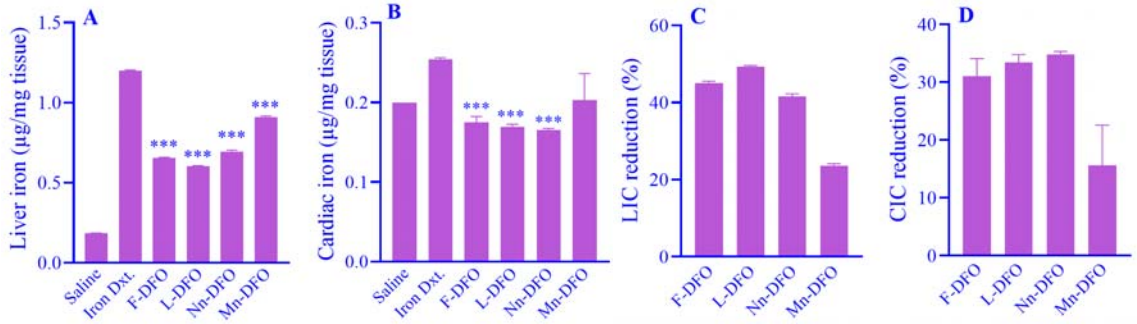

Fig. 8. Hepatic and cardiac iron concentration in mice receiving different deferoxamine formulations. Iron quantification was conducted by atomic absorption spectroscopy. (A) Liver iron, (B) cardiac iron, (C) percent reduction in liver iron compared to positive control, and (D) percent reduction in cardiac iron compared to positive control. Data are presented as mean + SD. ***$P \leq 0.001$ indicates significant differences compared to the positive control (Bonferroni post-hoc test). Iron Dxt, Iron dextran; F-DFO, free deferoxamine; L-DFO, liposomal deferoxamine; Mn-DFO, micro-niosomal deferoxamine; Nn-DFO, nano-niosomal deferoxamine; LIC, liver iron concentration; CIC, cardiac iron concentration.

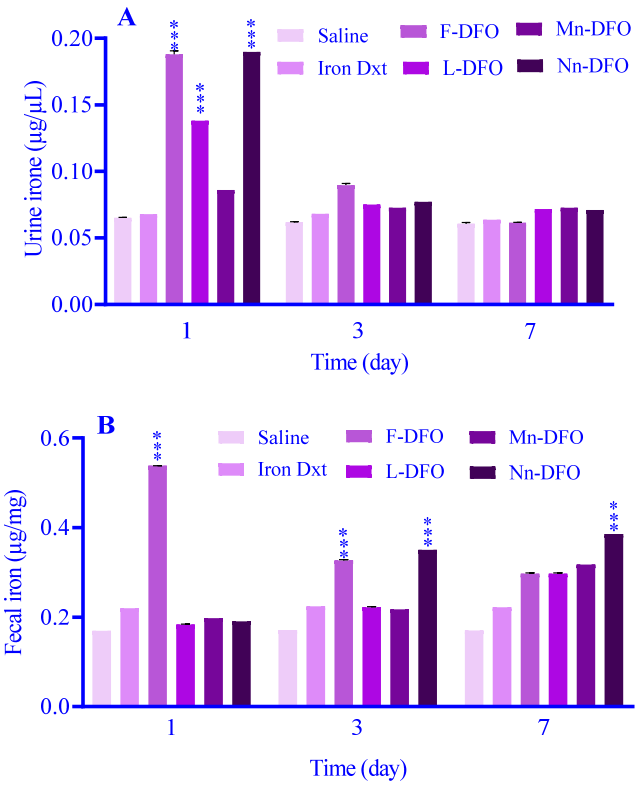

Fig. 9. Iron quantification in (A) urine and (B) fecal samples at 1, 3, and 7 days after the administration of the 5 doses of free or encapsulated DFO to iron overload mice. After 24 h post-administration, the highest urinary iron excretion belonged to the F-DFO and Nn-DFO groups. The F-DFO group showed the highest urinary iron excretion on day 3. On day 7, no significant difference was evident in urinary iron excretion between groups. Fecal excretion of iron within the first 24 h was the highest in the free DFO group. On day 3, fecal iron was the highest in the F-DFO and Nn-DFO groups. On day 7, the Nn-DFO group showed the highest fecal excretion of iron compared to the negative control. Data are presented as mean + SD. ***$P < 0.001$ indicates significant differences compared to the negative control. Iron Dxt, Iron dextran; F-DFO, free deferoxamine; L-DFO, liposomal deferoxamine; Mn-DFO, micro-niosomal deferoxamine; Nn-DFO, nano-niosomal deferoxamine.

DISCUSSION

In the present study, we used for the first time a microfluidic system to synthesize Nn-DFO and compare the formulation's physicochemical features, release profile, and iron chelating efficacy with liposomal and micro-niosomal carriers synthesized by the traditional thin film hydration method. Regarding the size of noisomes and liposomes encapsulated with DFO, the formulation synthesized by the microfluidic approach showed a lower mean particle diameter (87.06 ± 2.67 nm) compared to the formulations constructed by thin-film hydration (micro-niosomes: 9.04 ± 0.18 µm and liposomes: 180.89 ± 74.34 nm). DFO is a small molecule, and its half-life in circulation is relatively short due to rapid clearance by the kidneys. So, nano-constructs of DFO can elevate its size (from 5 nm in diameter to larger molecules up to micron-size), contributing to its longer circulatory half-life (12,26-32). Not only the plasma circulatory half-life of DFO nano-conjugates, but also their urinary excretion have been reported to be size-dependent (33). The size of nanocarriers must be optimized to obtain an appropriate pharmacokinetic balance, including distribution, half-life, degradation, and renal clearance. Ultra-large complexes of DFO, exceeding the filtration threshold of the kidneys, can increase the durability of the chelator in circulation (24,34). To pass through the kidney filtration barrier, nanomaterials must traverse three layers in the glomerular membrane: the endothelium with fenestrae

(70-90 nm), the meshwork glomerular basement membrane (with pores of 2-8 nm), and epithelium with filtration slits (4-11 nm) (35). Thus, to undergo primarily renal clearance, nanocarriers should be smaller than the kidney filtration threshold of around 6 nm while simultaneously avoiding sequestration by the phagocytic system mediated through protein opsonization. Therefore, a promising design strategy could encompass the fabrication of 10-100 nm particles able to gradually degrade into smaller particles near the renal clearance threshold, so guaranteeing as prolonged as possible circulatory half-life and acceptable removal rate from the body (36). Accordingly, the microfluidic approach seemed to render superiority in terms of the size of particles compared to liposomes and niosomes synthesized by thin-film hydration. As noted, the microfluidic approach allows rapid and scalable production of nanocarriers; however, there is a need for optimization of various synthetic parameters to achieve the desirable outcome in terms of particle size and other physicochemical properties (20).

An important aspect when it comes to nanocarriers is stability during storage. PDI, representing the homogeneity of size, and zeta potential, which shows the electric surface charge of particles, are two key parameters used for evaluating the stability of nano-based carriers. In the present study, the size stability of both liposomal and niosomal formulations was evaluated over 3 months, showing acceptable stability. Also, the PDIs observed for Nn-DFO and L-DFO were 0.47±0.01 and 0.39±0.05, respectively, which are below the recommended value of 0.7 as a plausible threshold (29). Also, compared to Mn-DFO (-3.45 mV) and L-DFO (-7.26 mV), the Nn-DFO synthesized by the microfluidic system showed a zeta potential of -38 mV, which is considered an optimal value. As a critical parameter, zeta potential affects not only size stability (by ensuring appropriate repulsion to prevent aggregation) but also the release behavior of liposomes and niosomes (*via* interactions with biological and environmental mediators and affecting the permeability of lipid layers). The repulsive forces in highly anionic or cationic colloidal systems prevent premature release of cargoes by keeping the integrity of the carrier, facilitating sustained and controlled release. On the other hand, particle aggregation in less stable colloidal systems such as liposomes and niosomes can disrupt membrane integrity and lead to premature drug release. Regarding size distribution and stability, the relatively small hydrodynamic diameter (~ 87 nm) and PDI (0.47) of Nn-DFO were consistent with the strong electrostatic repulsion (zeta potential of -38 mV) of these particles, indicating their plausible colloidal stability and low tendency for agglomeration, as evidenced in SEM images showing fairly separated and dispersed particles. According to their zeta potential values, L-DFO (-7.26 mV) and Mn-DFO (-3.45 mV) formulations seemed to have weak electrostatic stability, posing them at risk of aggregation and fusion; nevertheless, the size stability of these formulations was plausible over three months. This notion was further supported by the lack of significant aggregation in SEM and light microscopy images, respectively. Considering that zeta potential values between -10 to +10 mV are generally regarded as neutral and inadequate to prevent agglomeration of particles during storage (37), the zeta potential of -38 mV for Nn-DFO in this study surpassed this threshold, predicting desired stability. In a study by Marzban *et al*., the zeta potentials of free and DFO-encapsulated nano-niosomes were -18.2 ±5.1 mV and -13.2 ±4.5 mV, respectively, showing good stability over four months (12). In another study, liposomal structures with a zeta potential of -40 mV remained fairly stable over 50 days, while those with a zeta potential of +15 mV remained stable for nearly one month (29). A number of factors can influence surface charge and interactions in lipid-based carriers, including pH, ionic strength of the environment, lipid-solvent interactions, and hydrodynamic size. The near-neutral zeta potential observed in our micro-niosomes and liposomes might be partially explainable by the ions present in PBS, which was used as the solvent (38). Changes in pH can also lead to alterations in the protonation status of phospholipids and thereby influence their interactions with each other and chemical groups present in the environment (39).

The bioavailability of nano-encapsulated DFO largely depends on EE. In the present study, our results showed that the EE of Nn-DFO, Mn-DFO, and L-DFO for 3 mg/mL DFO were 57.1%, 70.72%, and 64.54%, respectively. Regarding the small size and hydrophilic nature of DFO, it seems that the higher EE of micro-niosomes compared to nano-niosomes and liposomes (70.72% *vs.* 57.1% and 64.54%) can be at least partially related to the larger aqueous space of the former (40). Further, the thin-film hydration technique has an inherent tendency for generating larger multilamellar vesicles, so more drug molecules can be entrapped into large multilamellar noisomes during the hydration phase (17), an argument that can also justify the slightly higher EE of liposomes compared to nano-niosomes (64.54% *vs.* 57.1%). In addition, this variation may also reflect the compositional differences between nano-niosomes and liposomes, where the surfactants used for the preparation of nano-niosomes could have led to more permeability of the membrane and drug leakage during preparation (41,42). Marzban *et al*. synthesized a noisome formulation of DFO using the combination of cholesterol, Span 20, Tween 80, and PEG 3000, reporting an EE of 96.8% (12), which probably highlights the impact of compositional structure on the loading capacity of lipid-based carriers. Lang *et al*. constructed liposomes co-carrying DFO and lificiguat (a hypoxia-inducible factor inhibitor 1α inhibitor, YC1), where the carrier was exposed to 100 mg DFO, reporting an EE of 21.3% (31), reflecting the effect of DFO mass on EE. In another study, Tran *et al*. synthesized liposomes containing cholesterol and either soy phosphatidylcholine (mean size: 88 nm) or palmitoyloleoylphosphatidylcholine (mean size: 119 nm) and reported that each mole of these lipid-based carriers could be loaded with 354 and 266 g of DFO, respectively, corresponding to 0.354 and 0.266 mg per µmol of liposomes (28). Therefore, the variable EEs reported in different studies can be explained by factors such as different ratios, molecular weights, and polarization of carriers' structural components, as well as drug solubility. All these modifiers can be better optimized in a well-defined microfluidic system rather than bulk synthesis methods.

Another important feature of a nano-based drug delivery system is gradual and sustained release, contributing to both prolonged circulatory half-life and effective renal clearance. This feature is of critical importance in nanocarriers loaded with iron chelators, considering the slow redistribution and mobilization of iron deposited in vital organs, where the iron and chelator must exhibit matched release kinetics. In the present experiment, DFO encapsulated within lipid-based nanocarriers showed a gradual release of 31.34%, 26.30%, and 20.95% of DFO from Nn-DFO, Mn-DFO, and L-DFO within 4 h, respectively. This was while 59.46% of DFO was released from F-DFO within 4 h. Toliyat *et al*. produced multivesicular liposomes containing DFO, reporting the gradual release of 60% of the loaded drug within nine days (43). In another study, niosomal DFO incorporated into nanofibers supported a controlled and sustained release of the drug for up to 9 days (44). Marzban *et al.* noted that DFO entrapped into niosomes showed a release of 5% within 2 h and 20% within 20 h (*vs*. 20% and 40% for free DFO, respectively) (12). In the case of DFO, the ability of the nanocarrier to support gradual release is logically essential for its optimal therapeutic efficacy. So, there is a need for reaching a functional balance since prolonged release periods (i.e., days or weeks) may reduce DFO chelating efficacy due to chemical instability of the drug, while rapid release could lead to its premature clearance and short circulatory or tissue half-life. Moreover, due to the relative toxicity and adverse effects of DFO, the gradual release of the drug further improves its safety profile and minimizes dose-related detrimental effects (45). As we observed, there was neither toxicity against erythrocytes *in vitro* nor renal or hepatic histological lesions in mice treated with the lipidic formulations carrying DFO, which aligned with previous reports noting a reduction in the toxicity of nano-encapsulated DFO (30,33,46-48).

Regarding therapeutic efficacy, we showed that all three nano-formulations preserved *in vitro* iron chelating activity compared to F-DFO and led to notable reductions in tissue iron content *in vivo* (liver: L-DFO: 49.36%, Nn-DFO: 41.63%, and Mn-DFO: 23.52%, *vs.*

F-DFO: 45.03% and heart: L-DFO: 33.39%, Nn-DFO: 34.77%, and Mn-DFO: 15.61%, *vs.* F-DFO: 31.02%). Likewise, Rossi *et al*. reported that the conjugation of DFO with polyethylene glycol methacrylate did not interfere with the *in vitro* chelating activity of the drug (13), and Tian *et al.* suggested that the complexation of DFO with alginate could preserve its iron chelation activity (49). In other studies, tissue iron reduction in mice models of hemochromatosis treated with 30-100 mg/kg deferasirox was from 8.4% to 63.1% and 38% for the liver, and from 10.6% to 49.1% for the heart (50). In iron-loaded gerbils, deferasirox reduced liver and cardiac iron content by 51% and 20.5% compared to 24.9% and 18.6% in animals treated with deferiprone (51). In a study conducted by Tran *et al*., liposomal DFO showed around 2-3-fold higher efficacy in removing iron from mouse models of iron overload (28). A niosomal formulation of DFO manufactured by Marzban *et al*. was also reported to efficiently chelate iron from hepatocytes *in vitro* (12). These results are in agreement with our observation, reflecting that the chelation activity of DFO could be either preserved or even enhanced after being conjugated with nano-polymeric compounds or encapsulated within nanocarriers such as liposomes and noisomes.

We further observed that Nn-DFO synthesized by the microfluidic system showed a superior immediate and delayed iron excretion profile compared to L-DFO, Mn-DFO, and F-DFO. There was a significant increase in immediate (i.e., day 1st) urinary iron excretion in all groups receiving DFO formulations, the highest being related to the F-DFO and Nn-DFO groups. Increased fecal iron excretion was observed on day 3rd in the F-DFO and Nn-DFO groups and on day 7th for the Nn-DFO group. Our results were consistent with previous reports on urinary and fecal iron excretion patterns reported for DFO and other chelators, such as DFX-loaded in various nanocarriers, including liposomes and niosomes (24,52-55). In iron overload conditions, the residency of iron chelators in the primary locations of iron accumulation (*e.g.,* liver) needs an appropriate size of the carrier so the urinary removal of the drug is logically delayed, and its circulatory half-life is likely extended (34). Our results supported a favorable shift in the pharmacokinetics and biodistribution of DFO encapsulated in nano-niosomes. Rather, the rapid clearance of F-DFO matches with the short half-life of the drug in circulation, in opposition to sustained-release Nn-DFO, possibly suggesting better targeting and accumulation of the recent in organs such as the liver. Consistently, lipidic nano-carriers are known for their protection of encapsulated drugs from rapid renal clearance, allowing for a stable reservoir of the drug (56). The tendency of the reticuloendothelial system for the uptake of lipid-based nano-carriers (57) or direct delivery of the drug *via* intracellular penetration (55) could lead to initial drug accumulation in organs such as the liver and spleen, followed by the subsequent release of DFO and delayed appearance in urine and feces.

Addressing the limitations of this study, we should acknowledge the small number of mice in each experimental group due to the fact that the goal of this pilot study was to gather preliminary data. Therefore, our results should be confirmed in studies with larger sample sizes. Another noteworthy point was that the EE of the Nn-DFO was determined by the dialysis membrane method, which differed from the centrifugation method used for L-DFO and Mn-DFO, leading to a slightly lower estimation of EE due to small remnants of the drug in nano-niosomes or diffusing out of some encapsulated drug during the test. Therefore, the direct comparison of EE between Nn-DFO and the two other formulations should be made with caution and interpreted in the context of this methodological variation. Further, we used the physicochemical factors of particle size, PDI, morphology, and EE as primary optimization factors; however, incorporating release properties as another key element in the optimization phase could offer a more robust roadmap. Finally, for better conclusions on the *in vivo* safety issue, our arguments could have been strengthened by analyzing biochemical markers of tissue damage.

CONCLUSION

In the present study, we employed the novel microfluidic system to synthesize Nn-DFO and investigate its physicochemical and functional

characteristics compared to liposomal and micro-niosomal carriers synthesized by traditional thin film hydration. Our results showed that the microfluidic approach could provide a rapid strategy for generating nano-niosomes with comparable and somehow superior physicochemical and functional features compared to lipidic carriers synthesized by the traditional method. A significant barrier limiting the clinical application of nano-encapsulated DFO is the lack of reproducibility and scalability of conventional bulk synthetic methods. The tiny-scale microfluidic approach can obviate limitations inherent to traditional synthesis techniques, enabling the production of functionally effective, structurally stable, and clinically applicable nano-carriers. The microfluidic technology allows for highly reproducible, scalable, and automated production of nano-formulations of drugs in terms of size, PDI, EE, release kinetics, and clinical efficacy by eliminating variations that are poorly controllable in traditional techniques. This is achieved by robust control on mixing conditions, tunable flow parameters, quality control attributes, and volume of materials, improving the scalability and cost-effectiveness, which are substantial requirements for clinical approval of drugs.

Acknowledgments

This was a part of a Ph.D. thesis carried out by Ali Bazi, which was financially supported by Kerman University of Medical Sciences through Grant No. 402000780 and National Institute for Medical Research Development through Grant No. 4020745. We would like to thank Mohammad Amin Raeisi Estabragh for his kind technical assistance.

Conflict of interest statement

All authors declared no conflict of interest in this study.

Authors' contributions

A. Bazi contributed to the concept, design, methodology, data analysis, and preparation and editing of the manuscript. S. Karami-Mohajeri was involved in animal studies, creating models, and interpreting the data. H. Mardani Valandani and F. Oroojalian participated in conceptualization and study design. E. Jafari contributed to histological analyses and interpreted pathological data. A. Pardakhty and R. Mirzaee Khalilabadi equally contributed to concept, design, methodology, supervision, resource provision, data interpretation, and revising the manuscript for important intellectual content. All authors have read and approved the finalized article. Each author has fulfilled the authorship criteria and affirmed that this article represents honest and original work.

Data availability

Data are readily available from the first and corresponding authors on a resealable request.

AI declaration

The authors did not use any AI-assisted technologies in the preparation of this manuscript.

REFERENCES

1. Yang A, Du L, Gao W, Liu B, Chen Y, Wang Y, *et al*. Associations of cortical iron accumulation with cognition and cerebral atrophy in Alzheimer's disease. Quant Imaging Med Surg. 2022;12(9):4570-5486. DOI: 10.21037/qims-22-7.
2. Zhou CH, Zhu YC. Imaging of cerebral iron as an emerging marker for brain aging, neurodegeneration, and cerebrovascular diseases. Brain Sci. 2025;15(9):944,1-19. DOI: 10.3390/brainsci15090944.
3. Mancardi D, Mezzanotte M, Arrigo E, Barinotti A, Roetto A. Iron overload, oxidative stress, and ferroptosis in the failing heart and liver. Antioxidants. 2021;10(12):1864,1-18. DOI: 10.3390/antiox10121864.
4. Tyagi P, Kumar A, Gupta D, Singh H. Decorporation of iron metal using dialdehyde cellulose-deferoxamine microcarrier. AAPS Pharm Sci Tech. 2017;18(1):156-165. DOI: 10.1208/s12249-016-0499-x.
5. Kontoghiorghes GJ. Iron load toxicity in medicine: from molecular and cellular aspects to clinical implications. Int J Mol Sci. 2023;24(16):12928. DOI: 10.3390/ijms241612928.
6. Entezari S, Haghi SM, Norouzkhani N, Sahebnazar B, Vosoughian F, Akbarzadeh D, *et al*. Iron chelators in treatment of iron overload. J Toxicol. 2022;2022(4):1-18. DOI: 10.1155/2022/4911205.
7. Hwang Y-F, Brown EB. Evaluation of deferoxamine in iron overload. Arch Intern Med. 1964;114(6):741-753. DOI: 10.1001/archinte.1964.03860120053003.
8. Huang V, Luini C, El-Ali A, Kessabi S. Iron chelation therapy: a review of the literature on the issues and importance of adherence to treatment in iron overload. Blood. 2015;126(23):4748. DOI: 10.1182/blood.V126.23.4748.4748.

9. Hamilton JL, Kizhakkedathu JN. Polymeric nanocarriers for the treatment of systemic iron overload. Mol and Cell Ther. 2015;3(1):3,1-15. DOI: 10.1186/s40591-015-0039-1.
10. Mukherjee S, Reddy A, Dutta N, Vaiphei KK, Vivek, Kumar A, *et al*. Exploring the potential of repurposed deferoxamine: bridging challenges and novel formulation opportunities. Nanomedicine. 2025: 20(16):2117-2141. DOI: 10.1080/17435889.2025.2534318.
11. Ghasemiyeh P, Mohammadi-Samani S. Solid lipid nanoparticles and nanostructured lipid carriers as novel drug delivery systems: applications, advantages and disadvantages. Res Pharm Sci. 2018;13(4):288-303. DOI: 10.4103/1735-5362.235156.
12. Marzban A, Akbarzadeh A, Ardestani MS, Ardestani F, Akbari M. Synthesis of nano-niosomal deferoxamine and evaluation of its functional characteristics to apply as an iron-chelating agent. Can J Chem Eng. 2018;96(1):107-112. DOI: 10.1002/cjce.23048.
13. Rossi NA, Mustafa I, Jackson JK, Burt HM, Horte SA, Scott MD, *et al*. *In vitro* chelating, cytotoxicity, and blood compatibility of degradable poly (ethylene glycol)-based macromolecular iron chelators. Biomaterials. 2009;30(4):638-648. DOI: 10.1016/j.biomaterials.2008.09.057.
14. Salimi A, Zadeh BSM, Kazemi M. Preparation and optimization of polymeric micelles as an oral drug delivery system for deferoxamine mesylate: *in vitro* and *ex vivo* studies. Res Pharm Sci. 2019;14(4):293-307. DOI: 10.4103/1735-5362.263554.
15. Bartelds R, Nematollahi MH, Pols T, Stuart MC, Pardakhty A, Asadikaram G, *et al*. Niosomes, an alternative for liposomal delivery. PLoS One. 2018;13(4):e0194179,1-18. DOI: 10.1371/journal.pone.0194179.
16. Amoabediny G, Haghiralsadat F, Naderinezhad S, Helder MN, Akhoundi Kharanaghi E, Mohammadnejad Arough J, *et al*. Overview of preparation methods of polymeric and lipid-based (niosome, solid lipid, liposome) nanoparticles:a comprehensive review. Int J Polym Mater Polym Biomater. 2018;67(3):383-400. DOI: 10.1080/00914037.2017.1332623.
17. Thabet Y, Elsabahy M, Eissa NG. Methods for preparation of niosomes:a focus on thin-film hydration method. Methods. 2022;199:9-15. DOI: 10.1016/j.ymeth.2021.05.004.
18. Ag Seleci D, Maurer V, Stahl F, Scheper T, Garnweitner G. Rapid microfluidic preparation of niosomes for targeted drug delivery. Int J Mol Sci. 2019;20(19):4696,1-12. DOI: 10.3390/ijms20194696.
19. Aljabali AA, Tambuwala MM, Obeid MA. Microfluidic manufacturing of niosomes. Microfluidics in Pharmaceutical Sciences. 2024:77-108. DOI: 10.1007/978-3-031-60717-2_4.
20. Obeid MA, Khadra I, Aljabali AA, Amawi H, Ferro VA. Characterisation of niosome nanoparticles prepared by microfluidic mixing for drug delivery. Int J Pharm X. 2022;4:100137,1-7. DOI: 10.1016/j.ijpx.2022.100137.
21. Shokoohinia P, Hajialyani M, Sadrjavadi K, Akbari M, Rahimi M, Khaledian S, *et al*. Microfluidic-assisted preparation of PLGA nanoparticles for drug delivery purposes: experimental study and computational fluid dynamic simulation. Res Pharm Sci. 2019;14(5):459-470. DOI: 10.4103/1735-5362.268207.
22. Alam MK. Nanocarrier-based drug delivery systems using microfluidic-assisted techniques. Adv NanoBiomed Res. 2023;3(11):2300041,1-38. DOI: 10.1002/anbr.202300041.
23. Liu Z, Lin TM, Purro M, Xiong MP. Enzymatically biodegradable polyrotaxane–deferoxamine conjugates for iron chelation. ACS Appl Mater Interfaces. 2016;8(39):25788-25797. DOI: 10.1021/acsami.6b09077.
24. Hamilton JL, Imran ul-haq M, Abbina S, Kalathottukaren MT, Lai BF, Hatef A, *et al. In vivo* efficacy, toxicity and biodistribution of ultra-long circulating desferrioxamine based polymeric iron chelator. Biomaterials. 2016;102:58-71. DOI: 10.1016/j.biomaterials.2016.06.019.
25. Uddin AH, Khalid RS, Alaama M, Abdualkader AM, Kasmuri A, Abbas S. Comparative study of three digestion methods for elemental analysis in traditional medicine products using atomic absorption spectrometry. J Anal Sci Technol. 2016;7(1):6,1-7. DOI: 10.1186/s40543-016-0085-6.
26. Al Sabaa H, Mady FM, Hussein AK, Abdel-Wahab HM, Ragaie MH. Dapsone in topical niosomes for treatment of acne vulgaris. Afr J Pharm Pharmacol. 2018;12(18):221-230. DOI: 10.5897/AJPP2018.4925.
27. El-Say KM, Abd-Allah FI, Lila AE, Hassan AE-SA, Kassem AEA. Diacerein niosomal gel for topical delivery: development, *in vitro* and *in vivo* assessment. J Liposome Res. 2016;26(1):57-68. DOI: 10.3109/08982104.2015.1029495.
28. Tran DT, Hayes ME, Noble CO, Dai Z, Working PK, Szoka FC. Twice monthly liposome encapsulated deferoxamine (LDFO) has a high molar efficiency in removing total body iron in an iron dextran-overloaded mouse model. Blood. 2016;128(22):2322-2225. DOI: 10.1182/blood.V128.22.2322.2322.
29. Ribeiro CM, Roque-Borda CA, Franzini MC, Manieri KF, Demarqui FM, Campos DL, *et al*. Liposome-siderophore conjugates loaded with moxifloxacin serve as a model for drug delivery against Mycobacterium tuberculosis. Int J Pharm. 2024;655:124050. DOI: 10.1016/j.ijpharm.2024.124050.
30. Guo S, Liu G, Frazer DM, Liu T, You L, Xu J, *et al*. Polymeric nanoparticles enhance the ability of deferoxamine to deplete hepatic and systemic iron. Nano Lett. 2018;18(9):5782-5790. DOI: 10.1021/acs.nanolett.8b02428.
31. Lang J, Zhao X, Wang X, Zhao Y, Li Y, Zhao R, *et al*. Targeted co-delivery of the iron chelator deferoxamine

and a HIF1α inhibitor impairs pancreatic tumor growth. ACS nano. 2019;13(2):2176-2189. DOI: 10.1021/acsnano.8b08823.
32. Barani M, Sargazi S, Hajinezhad MR, Rahdar A, Sabir F, Pardakhty A, *et al*. Preparation of pH-responsive vesicular deferasirox: evidence from *in silico, in vitro*, and *in vivo* evaluations. ACS omega. 2021;6(37):24218-24232. DOI: 10.1021/acsomega.1c03816.
33. Jones G, Goswami SK, Kang H, Choi HS, Kim J. Combating iron overload: a case for deferoxamine-based nanochelators. Nanomedicine. 2020;15(13):1341-1356. DOI: 10.2217/nnm-2020-0038.
34. Hoshyar N, Gray S, Han H, Bao G. The effect of nanoparticle size on *in vivo* pharmacokinetics and cellular interaction. Nanomedicine. 2016;11(6):673-692. DOI: 10.2217/nnm.16.5.
35. Gong L, Wang Y, Liu J. Bioapplications of renal-clearable luminescent metal nanoparticles. Biomater Sci. 2017;5(8):1393-1406. DOI: 10.1039/C7BM00257B.
36. Zhu GH, Gray AB, Patra HK. Nanomedicine: controlling nanoparticle clearance for translational success. Trends Pharmacol Sci. 2022;43(9):709-711. DOI: 10.1016/j.tips.2022.05.001.
37. Clogston JD, Patri AK. Zeta potential measurement. Methods Mol Biol. 2011:697:63-70. DOI: 10.1007/978-1-60327-198-1_6.
38. Liang H, Zou F, Liu Q, Wang B, Fu L, Liang X, *et al*. Nanocrystal-loaded liposome for targeted delivery of poorly water-soluble antitumor drugs with high drug loading and stability towards efficient cancer therapy. Int J Pharm. 2021;599:120418,1-16. DOI: 10.1016/j.ijpharm.2021.120418.
39. Sułkowski W, Pentak D, Nowak K, Sułkowska A. The influence of temperature, cholesterol content and pH on liposome stability. J Mol Struct. 2005;744:737-747. DOI: 10.1016/j.molstruc.2004.11.075.
40. Akbarzadeh A, Rezaei-Sadabady R, Davaran S, Joo SW, Zarghami N, Hanifehpour Y, *et al*. Liposome: classification, preparation, and applications. Nanoscale Res Lett. 2013;8(1):102,1-9. DOI: 10.1186/1556-276X-8-102.
41. Manosroi A, Wongtrakul P, Manosroi J, Sakai H, Sugawara F, Yuasa M, *et al*. Characterization of vesicles prepared with various non-ionic surfactants mixed with cholesterol. Colloids Surf B Biointerfaces. 2003;30(1-2):129-138. DOI: 10.1016/S0927-7765(03)00080-8.
42. Moghassemi S, Hadjizadeh A. Nano-niosomes as nanoscale drug delivery systems: an illustrated review. J Control Release. 2014;185:22-36. DOI: 10.1016/j.jconrel.2014.04.015.
43. Toliyat T, Jorjani M, Khorasanirad Z. An extended-release formulation of desferrioxamine for subcutaneous administration. Drug Deliv. 2009;16(7):416-421. DOI: 10.1080/10717540903141768.
44. Nour S, Imani R, Mehrabani M, Solouk A, Iranpour M, Jalili-Firoozinezhad S, *et al*. Biomimetic hybrid scaffold containing niosomal deferoxamine promotes angiogenesis in full-thickness wounds. Mater Today Chem. 2023;27:101314. DOI: 10.1016/j.mtchem.2022.101314,1-19.
45. Agboluaje EO, Cui S, Grimsey NJ, Xiong MP. Bile acid–targeted hyaluronic acid nanoparticles for enhanced oral absorption of deferoxamine. AAPS J. 2024;26(3):46. DOI: 10.1208/s12248-024-00911-z.
46. Zhu F, Zhong J, Hu J, Yang P, Zhang J, Zhang M, *et al*. Carrier-free deferoxamine nanoparticles against iron overload in brain. CCS Chem. 2023;5(1):257-270. DOI: 10.31635/ccschem.022.202101696.
47. Abbina S, Abbasi U, Gill A, Wong K, Kalathottukaren MT, Kizhakkedathu JN. Design of safe nanotherapeutics for the excretion of excess systemic toxic iron. ACS Cent Sci. 2019;5(5):917-926. DOI: 10.1021/acscentsci.9b00284.
48. Imran ul-haq M, Hamilton JL, Lai BF, Shenoi RA, Horte S, Constantinescu I, *et al*. Design of long circulating nontoxic dendritic polymers for the removal of iron *in vivo*. ACS Nano. 2013;7(12):10704-10716. DOI: 10.1021/nn4035074.
49. Tian M, Chen X, Gu Z, Li H, Ma L, Qi X, *et al*. Synthesis and evaluation of oxidation-responsive alginate-deferoxamine conjugates with increased stability and low toxicity. Carbohydr Polym. 2016;144:522-530. DOI: 10.1016/j.carbpol.2016.03.014.
50. Nick H, Allegrini PR, Fozard L, Junker U, Rojkjaer L, Salie R, *et al*. Deferasirox reduces iron overload in a murine model of juvenile hemochromatosis. Exp Biol Med. 2009;234(5):492-503. DOI: 10.3181/0811-rm-337.
51. Wood JC, Otto-Duessel M, Gonzalez I, Aguilar MI, Shimada H, Nick H, *et al*. Deferasirox and deferiprone remove cardiac iron in the iron-overloaded gerbil. Transl Res. 2006;148(5):272-280. DOI: 10.1016/j.trsl.2006.05.005.
52. Kang H, Han M, Xue J, Baek Y, Chang J, Hu S, *et al*. Renal clearable nanochelators for iron overload therapy. Nat Commun. 2019;10(1):5134,1-11. DOI: 10.1038/s41467-019-13143-z.
53. Wang Y, Liu Z, Lin TM, Chanana S, Xiong MP. Nanogel-DFO conjugates as a model to investigate pharmacokinetics, biodistribution, and iron chelation *in vivo*. Int J Pharm. 2018;538(1-2):79-86. DOI: 10.1016/j.ijpharm.2018.01.004.
54. Guilmette R, Cerny E, Rahman YJLS. Pharmacokinetics of the iron chelator desferrioxamine as affected by liposome encapsulation: potential in treatment of chronic hemosiderosis. Life Sci. 1978;22(4):313-320. DOI: 10.1016/0024-3205(78)90138-8.
55. Lau EH, Cerny EA, Rahman YE. Liposome-encapsulated desferrioxamine in experimental iron overload. Br J Haematol. 1981;47(4):505-518. DOI: 10.1111/j.1365-2141.1981.tb02679.x.
56. Kesharwani R, Jaiswal P, Patel DK, Yadav PK. Lipid-based drug delivery system (LBDDS): an emerging paradigm to enhance oral bioavailability of poorly soluble drugs. Biomed Mater Devices. 2023;1(2):648-663. DOI: 10.1007/s44174-022-00041-0.
57. Zhao YQ, Li LJ, Zhou EF, Wang JY, Wang Y, Guo LM, *et al*. Lipid-based nanocarrier systems for drug delivery: advances and applications. Pharm Fronts. 2022;4(02):e43-e60. DOI: 10.1055/s-0042-1751036.